A Navigational Primitive: Biorobotic Implementation of Cycloptic Helical Klinotaxis in Planar Motion

John H. Long, Jr., *Member, IEEE*, Adam C. Lammert, Charles A. Pell, Mathieu Kemp, James A. Strother, Hugh C. Crenshaw, and Matthew J. McHenry

***Abstract*—A broad diversity of microorganisms and larval aquatic animals swim along a helical trajectory. Helical movement toward or away from stimuli involves the detection of gradients, alteration of the helical trajectory, and gradient tracking. Using sensory and neural circuitry models from swimming simulations of tadpole-like ascidian larvae (Phylum Chordata, Subphylum Urochordata), we built and tested a single-sensor, surface-swimming, tail-flapping robot that swims up a light gradient and holds station at an orbital around an area of high intensity. We implemented the same neural circuitry in a terrestrial, wheeled robot with a single photoresistor; it exhibited similar navigational behavior. We also mathematically modeled single-sensor robots navigating in plane. The simulated robots showed the importance of sensor placement and excitation field on navigational behavior. When the sensor placement and excitation field of the simulated robot matched that of the embodied robots, navigational behavior was similar. These results 1) tested and supported a proposed neural circuitry model, 2) showed the simplicity and effectiveness of using a single light sensor for navigation, and 3) demonstrated the use of helical motion in two dimensions.**

***Index Terms*—Aquatic vehicles, behavior-based robotics, navigation, neural control.**

I. Introduction

OUR goal is to find, adapt, and implement a biological schema—"a basic unit of behavior from which complex actions can be constructed" [1]—for planar navigational control in aquatic autonomous underwater vehicles (AUVs). In particular, we are interested in developing navigational primitives, irreducible schema building blocks that can be used in a variety of systems and mission-specific conditions [2]. Our initial focus is on planar (2-D) motion in AUVs for several reasons.

1) Its kinematics and dynamics are simpler [fewer degrees of freedom (DOFs)] than those of volumetric (3-D) motion.
2) Its development for biorobotic AUVs lags behind that for 3-D AUVs [3], [4].
3) Its use is suitable for surface vehicles, roll-stable AUVs maneuvering in any plane, and amphibious AVs working in 2-D near-shore aquatic and terrestrial environments.

A. Directional Navigation With One Sensor

Our quest for a navigational primitive begins with single-sensor systems. A proof-of-concept for single-sensor navigation is provided by biology. The tadpole-like larvae of ascidians (Phylum Chordata, Subphylum Urochordata, $\sim$3 mm total length; Fig. 1) swim toward and away from light ("phototaxis") at low and intermediate Reynolds numbers (Re<100). They do so using a single eye-spot and a 3-D helical trajectory [5], [6]. The combined sensory-motor schema provides the tadpole-like larva with the ability to detect gradients and to navigate with respect to them [7]. The resulting 3-D navigational behavior is called helical klinotaxis (HK), where "klinotaxis" refers strictly to orientation by use of vector information [8]. HK is widespread in a variety of intermediate- and low-Re swimming organisms [9]–[13], suggesting that natural selection has repeatedly generated and/or conserved this simple and robust navigational schema. We refer to HK with a single sensor as cycloptic HK (cHK).

Ground-breaking use of 3-D cHK for the operation of micro-AUVs has been accomplished by Nekton Research (Durham, NC). A submersible, Microhunter, navigates with a single propeller that adjusts the helical trajectory by modulating propeller speed [3], [4], which, in turn, alters the vehicle's translational and rotational velocity vectors [14]. With two vectors necessary for control, Microhunter has revealed that 3-D cHK has more complex dynamics than that predicted from kinematics alone [9]–[11]. Likewise, treating 2-D HK as a simple, special case of 3-D HK [12] may overlook important operational dynamics of embodied systems. To extend our understanding of 2-D cHK, we combined robotic experiments and mathematical analysis.

B. Neural Control Circuit for cHK in Ascidian Larvae

A schema includes the neurocomputational rules that link changes in sensor readings to changes in motor output [1]. Four sets of schema rules (roughly "neural circuits") for the control of 3-D cHK were tested in a physics-based simulation of the tadpole-like larvae of ascidians [7]. Each neural circuit linked the tadpole's single eyespot ("ocellus") to muscles that offset the lateral orientation of the flapping tail to the right or the left of the body. The simplest circuit that produced realistic phototactic behavior—and the circuit that we used in our robots—changed

Manuscript received September 30, 2003. This work was supported in part by the U.S. National Science Foundation under Grant BCS-0320764.

J. H. Long, Jr., and A. C. Lammert are with the Program in Cognitive Science and Department of Biology, Vassar College, Poughkeepsie, NY 12604 USA (e-mail: jolong@vassar.edu; adlammert@vassar.edu).

C. A. Pell and M. Kemp are with Nekton Research LLC, Durham, NC 27713 USA (e-mail: cap@nektonresearch.com; fruitbat@nektonresearch.com).

J. A. Strother is with the Department of Integrative Biology, University of California, Berkeley, CA 94720 USA (e-mail: strother@socrates.berkeley.edu).

H. C. Crenshaw is with the Technology Development Department, GlaxoSmithKline, Research Triangle Park, NC 27709 USA (e-mail: hugh.c.crenshaw@gsk.com).

M. J. McHenry is with the Department of Organismic and Evolutionary Biology, Harvard University, Cambridge, MA 02138 USA (e-mail: mchenry@fas.harvard.edu).

Digital Object Identifier 10.1109/JOE.2004.833233

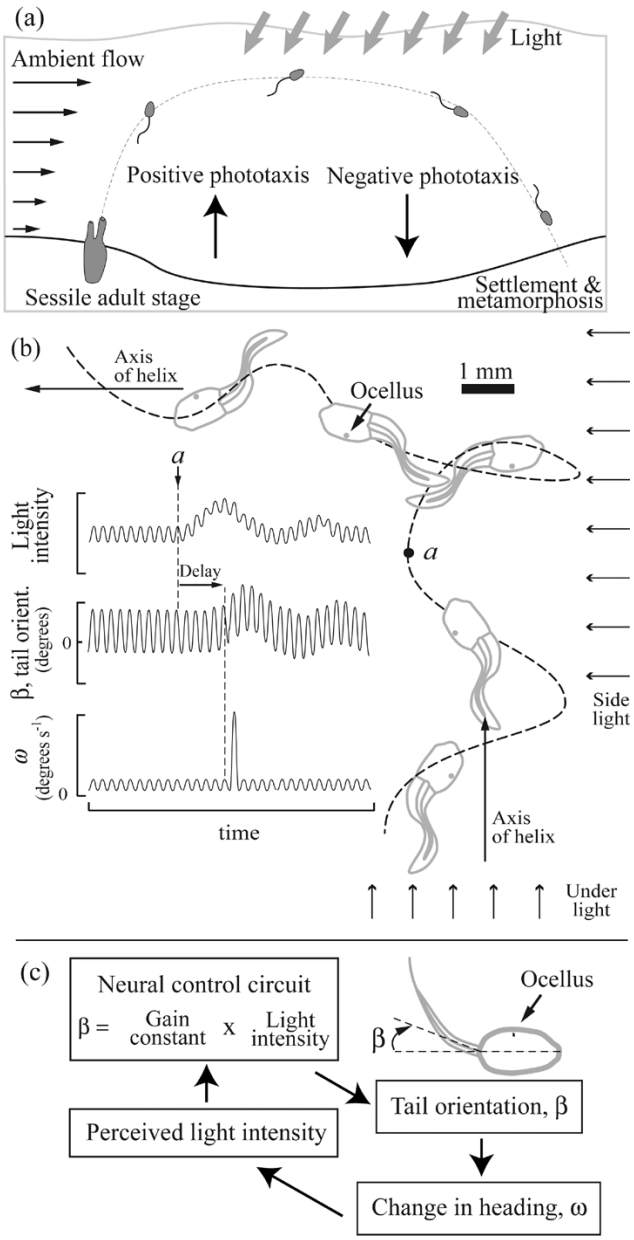

Fig. 1. Single-sensor, phototaxic navigation (3-D cHK) in tadpole-like larvae of ascidians (Phylum Chordata; Subphylum Urochordata). (a) Larval life stage. Upon release from the benthic adult, a larva swims up toward the light (positive phototaxis), into the water column, where it is dispersed by ambient flow. Later, the larva swims down away from the light (negative phototaxis) to settle on the substrate. (b) Single-sensor control of helical trajectory. An experimental change in the direction of illumination (from "under" to "side" light at "a") causes a slow oscillation in perceived light intensity at the ocellus, which triggers an asymmetry in tail beating (nonzero lateral tail orientation β). The change in lateral orientation of the tail causes a change in heading (rotational velocity) ω that in turn alters the orientation of the body and direction of the axis of the helical trajectory [6]. (c) Neural control circuit. The lateral orientation β of the beating tail is hypothesized to be proportional to perceived light intensity and is continuously adjusted in a feedback loop.

the tail's lateral orientation β in proportion to the intensity of light sampled by the ocellus (Fig. 1). The β, in turn, controlled the curvature of the animal's path, given a constant translational velocity, by varying the rotational velocity of the body ω.

C. Implementation

To examine the performance and control of 2-D cHK, we built a surface-swimming robotic tadpole that navigates up a light intensity gradient (Fig. 2). The robotic tadpole uses a single photoresistor coupled to the lateral orientation motor of a flapping tail by way of an analog circuit that instantiates the 3-D cHK neural circuit for tadpole-like ascidian larvae. Changes in light intensity at the photoresistor cause proportional changes in the lateral orientation, β, of the propulsive flapper (Fig. 2). To test the generality of the 2-D cHK navigational primitive, we implemented it on a terrestrial robot with a digital control system.

To establish a theoretical understanding, we numerically modeled the kinematics of a 2-D cHK robot in vector fields of constant and spatially varying excitation. We also explored the influence of the position of the sensor on robot behavior.

II. Methods

A. Surface-Swimming Robotic Tadpole

The hull of the robotic tadpole (Fig. 2) was a keelless displacement type, made of plastic, with a circular, flat bottom and slightly flared topsides (Rubbermaid, 1.4 l). This shape was chosen as a first approximation of the bulbous anterior section of the tadpole-like ascidian larva (see Fig. 1). With ballast, batteries, electronics, and attached stern drive, the robot displaced 850 ± 100 cm^2 (± 1 standard deviation) of water. The robot's length (diameter) on the waterline (LWL) was 15.8 cm, its draft was 6.2 cm, and its freeboard was 4.8 cm. During experiments, the Reynolds number of the robot, using LWL as the characteristic length, ranged from 1580 to 14 200, more than three orders of magnitude greater than that of actual tadpole-like ascidian larvae [15].

The robotic tadpole was propelled by a laterally oscillating tail driven at a constant frequency, 2.00 ± 0.04 Hz (± 1 st. dev.), and amplitude, 5.43 ± 0.18 cm (± 1 standard deviation), by a rotary motor (1.5 VDC; single AA battery) attached to a reduction gear box and sliding crank [Fig. 2(c)]. Because of the asymmetry inherent in the sliding crank, tail motion was temporally asymmetric, such that motion to one side took slightly longer than that to the opposite side. The terminal tail blade was made of duct tape fashioned into a rectangular element of 6.7 cm length $\times$ 3.6 cm height $\times$ 0.1 cm thickness.

The propulsive unit's lateral orientation β was driven by a separate rudder motor (20 kΩ motorized potentiometer; single 9 VDC battery; Shokai model WHE1604A) attached to the hull and the propulsive system (Fig. 2). The magnitude and sign of β was determined continuously by negative feedback in an analog circuit (Fig. 3) that coupled the rudder motor's lateral orientation to the input from a photoresistor. The single photoresistor (20 kΩ) was the sole sensory input, and it was mounted at an angle δ relative to the robot's centerline, of 45°. A digital panel meter [3.5 digit panel meter with liquid crystal display (LCD)] displayed the voltage across the photoresistor in real time. A pair of operational amplifiers (LM741) acted as voltage comparators. When the voltages from the sensor and the motor were equal, neither comparator produced an output and β remained unchanged. However, when the photoresistor's voltage changed in response to a different light intensity, one of the comparators produced a high voltage output, generating, by way of the relays, a change in the polarity and/or or power reaching the rudder motor. The operational range of β was approximately

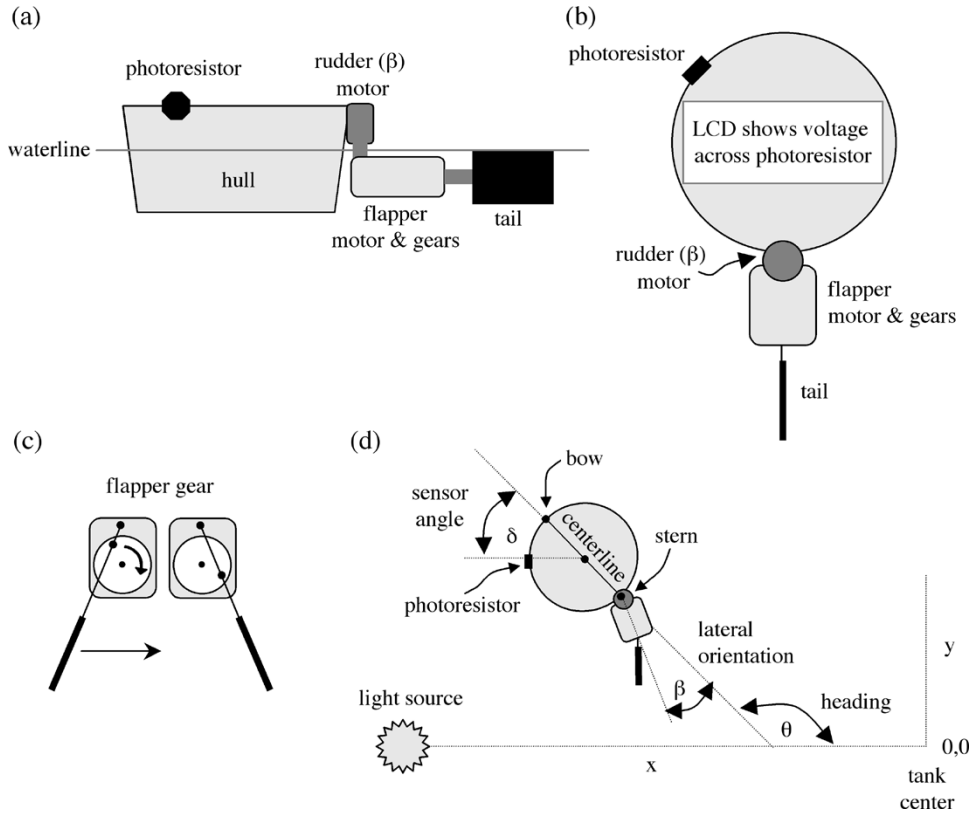

Fig. 2. Design of the autonomous surface-swimming robotic tadpole. (a) Side view. (b) Top view. (c) The flapper gear, showing extreme lateral positions of tail. (d) Coordinate system and definition of robot heading θ, lateral orientation of tail β, and sensor angle δ.

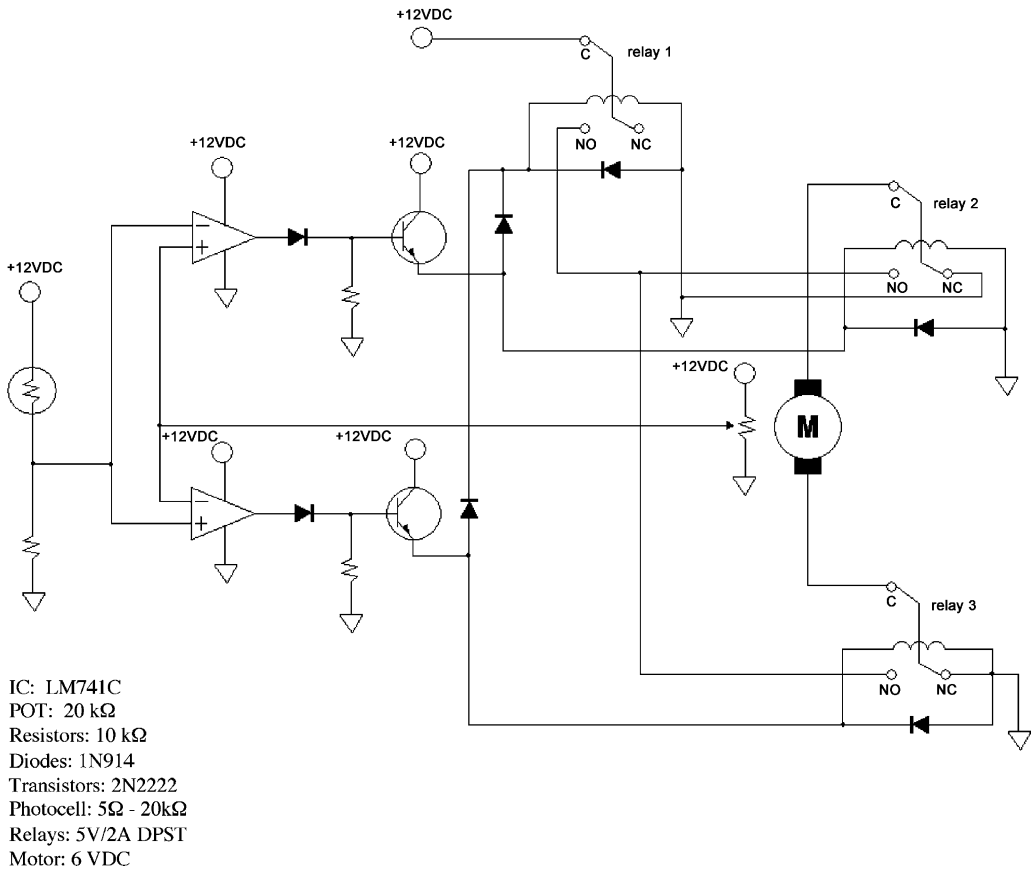

Fig. 3. Analog cHK control circuit for the robotic tadpole. The circuit couples light intensity at the photoresistor to the position of the rudder motor (M), which, in turn, controls the lateral orientation of the tail (β; see Fig. 2).

$\pm 100^{\circ}$, and, during dark experimental conditions, the position of the propulsive unit was to the right side, causing the robot to swim in circles when not sensing light.

B. Terrestrial Robot

We used the Rug Warrior Pro Mobile Robot Kit (A. K. Peters, Ltd.). The Rug Warrior had a circular body with a 20 cm diameter, a differential drive to two wheels, and a digital microcontroller that was programmable using the Interactive C language. We disabled all sensors except the left photoresistor, which had a similar angular position, $\delta = 45^{\circ}$, as the aquatic robot.

The coupling of photoresistor and motor output was implemented using the Interactive C programming language:

```
void main () {
  int omega;
  init_motors ();
  while (1) {
    sleep (.050);
    omega = ((analog(1) - 20)*2);
    if (omega > 36)
      omega = 36;
    if (omega < -36)
      omega = -36;
  printf ("rotational vector is %d\n");
  drive (50, omega); }}
```

The library functions included one called "drive()," which takes two arguments, the translational speed and the rotational vector. We coded the translational speed as a constant (50, above) and the rotational vector as a simple output, omega, of a windowed linear function whose input is the photoresistor voltage, analog(1). A gain value of two was used. The program also printed the rotational speed on Rug Warrior's LCD.

C. Experiments

We created two different light environments for testing the navigational abilities of the surface-swimming robotic tadpole. In the first, called "spotlight condition," a testing environment was created using a circular tank of diameter 1.82 m that was filled with water to a height of 0.15 m. A light source was positioned 1.00 m above the water level, and 0.21 m inside the rim of the tank. Light was provided by a 125 W incandescent spot bulb pointed perpendicular to the water surface. A light gradient was created with the point of highest intensity being 10 660 lux, as measured directly under the bulb at the water line with a digital photometer (Spectra model Professional IV-A). The intensity of light on the opposite side of the tank was 144 lux. The intervening decrease in light was characteristically proportional to the inverse square of distance. The robot was placed in the tank with the spotlight off. After the vehicle rotated three times, we turned on the light. The experiment ceased after the robot had oriented toward the point of maximal intensity, navigated in that direction, and held station around that point for three rotations. To control for the influence of the cHK neural circuit, we also ran experiments with the circuit off-line.

In the second light environment, called the "threshold condition," we divided the tank into halves and held one side dark and the other light without a spot of highest intensity. The light was positioned above the tank rim at a height of 0.80 m above the water. Unlike the first environment, in which the light was turned on during the experiment, in this case the lighting conditions remained constant. The experiment began by placing the robot into the dark section facing away from the light side. The experiment ended after the robot had oriented toward the light side, navigated toward that side, and completed three rotations in the light side.

It is important to note that the walls of the tank restricted the motion of the robotic tadpole at times in both sets of experiments. In spite of these interactions, we still had a strong correlation between light intensity and change in the heading of the craft (see Section III).

A final set of two experiments was conducted using the Rug Warrior robot under the spotlight condition. The same protocol was followed as outlined above, except that the trial was conducted in an arena without walls, and the light source was positioned at 0.71 m above the plane of movement. In the first three trials, the speed vector was set at 35 (arbitrary motor units). At this magnitude, the robot rotated around its right wheel in the dark. In the second set of three trials we increased the speed vector to 50, which increased the radius of the rotational motion.

All experiments were repeated three times and recorded using two digital video camcorders (Panasonic GRL-500); one captured the robot's movements around the whole tank or arena and one followed the LCD readout of the voltage across the photoresistor. We calibrated the photoresistor's voltage to light intensity using a digital photometer.

From the video images, two marked points on the bow and stern of the robots, representing the centerline [Fig. 2(d)], were tracked through time and space using motion-analysis software (VideoPoint) on a Macintosh computer. For each image, the points were used to calculate a midpoint corresponding to the center of the circular robots; the robots' centers were used to plot trajectories. Spatial coordinates were taken with respect to a Cartesian coordinate system with the origin at the center of the tank [Fig. 2(d)]. The x-axis extended through the light source in the negative direction. The heading of the robot θ was measured in each image as the angle of the robots' centerline with respect to the external coordinate system. An orientation parallel to the x-axis with the stern facing the light source was a θ of 0°. Also calculated was the change in heading with respect to time ω [deg/(5 s)] at 5 s increments on the video; this is a measure of angular velocity.

D. Mathematical Modeling of Simulated Robots

We modeled the 2-D kinematics of the cHK robots by tracking the center of the simulated robot at (x, y). The heading of the robot's body was θ; it increased counterclockwise and was 0° when the robot pointed along the x-axis. The speed of the robot was $\mathrm{U}(\cos\theta, \sin\theta)$ and was held constant at 0.2 m s^{-1}. The angular velocity ω was modulated linearly by the external signal, and the sensor was described by a normalized vector S normal to its plane: $S = (\cos(\theta + \delta), \sin(\theta + \delta))$,

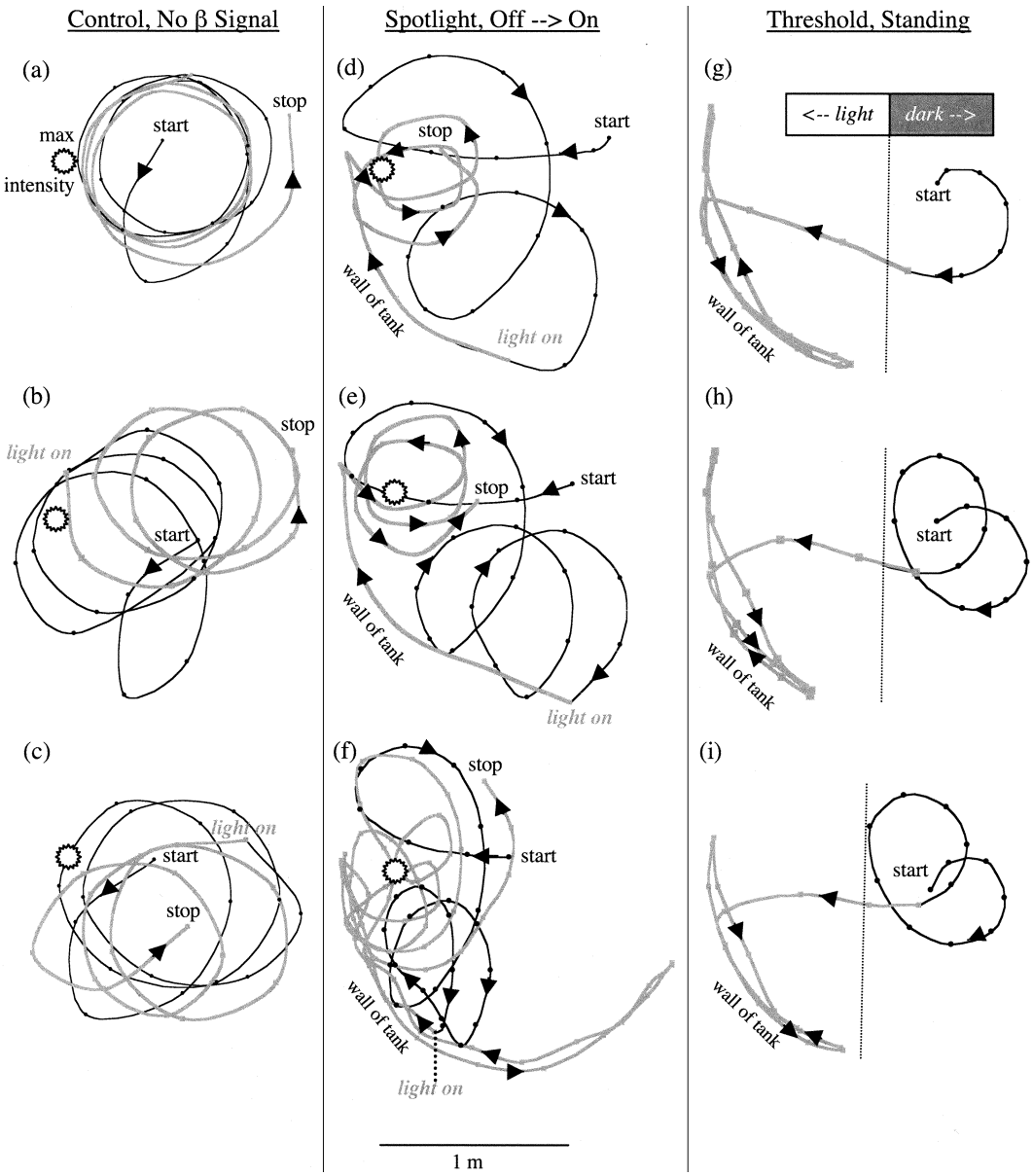

Fig. 4. Trajectories of the surface-swimming robotic tadpole under three different experimental conditions, with start and stop positions indicated. For the control and spotlight experiments, the time when the light was turned on is indicated as the transition point from a black to gray line. In those same experiments, the sun symbol shows the position on the surface of the water of maximal light intensity. In the threshold experiments, the boundary between dark and light conditions is demarcated by the dashed vertical line. The wall of the tank is indicated where the path of the robot is constrained by it. Arrows indicate forward motion.

where δ is the angle between the sensor and robot's centerline. The equations of motion for the robot were

$$\frac{dX}{dt} = U(\cos\theta, \sin\theta), \quad \frac{d\theta}{dt} = \omega. \tag{1}$$

We started with a field of constant excitation described by the vector $V = (-f_0, 0)$. The angular velocity was

$$\omega = \alpha(V \bullet S - T_0) = -\alpha\left(f_0 \cos(\theta + \delta) + T_0\right) \tag{2}$$

where α was the HK gain and $T_o (< f_o)$ was the threshold intensity at which the angular velocity changed direction. Of the two robot orientations where ω was zero, one was an attractor which we denoted by θ_+. The function $(\theta - \theta_+)^2$ was a Lyapunov function [16]

$$\frac{d(\theta - \theta_+)^2}{dt} = 2(\theta - \theta_+)\omega \leq 0 \tag{3}$$

because ω was negative whenever $(\theta - \theta_+)$ was positive and vice-versa. Because the Lyapunov function was decreasing, the robot's trajectory converged on θ and stayed there.

Next we generalized this result for the case of a spatially varying excitation field. We considered a radial source

$$V = -f(r)\frac{(x, y)}{r} \tag{4}$$

i.e., a vector field that pointed toward the source and whose intensity depended on distance. We used the same control law as above (2). To a good approximation, the result found above was applicable locally provided the field varied slowly; i.e., provided $|\nabla\varphi| U\tau \ll 1$ where τ was the Lyapunov relaxation time. Under this "adiabatic" condition, the robot constantly adjusted its heading θ in order to null its angular velocity ω.

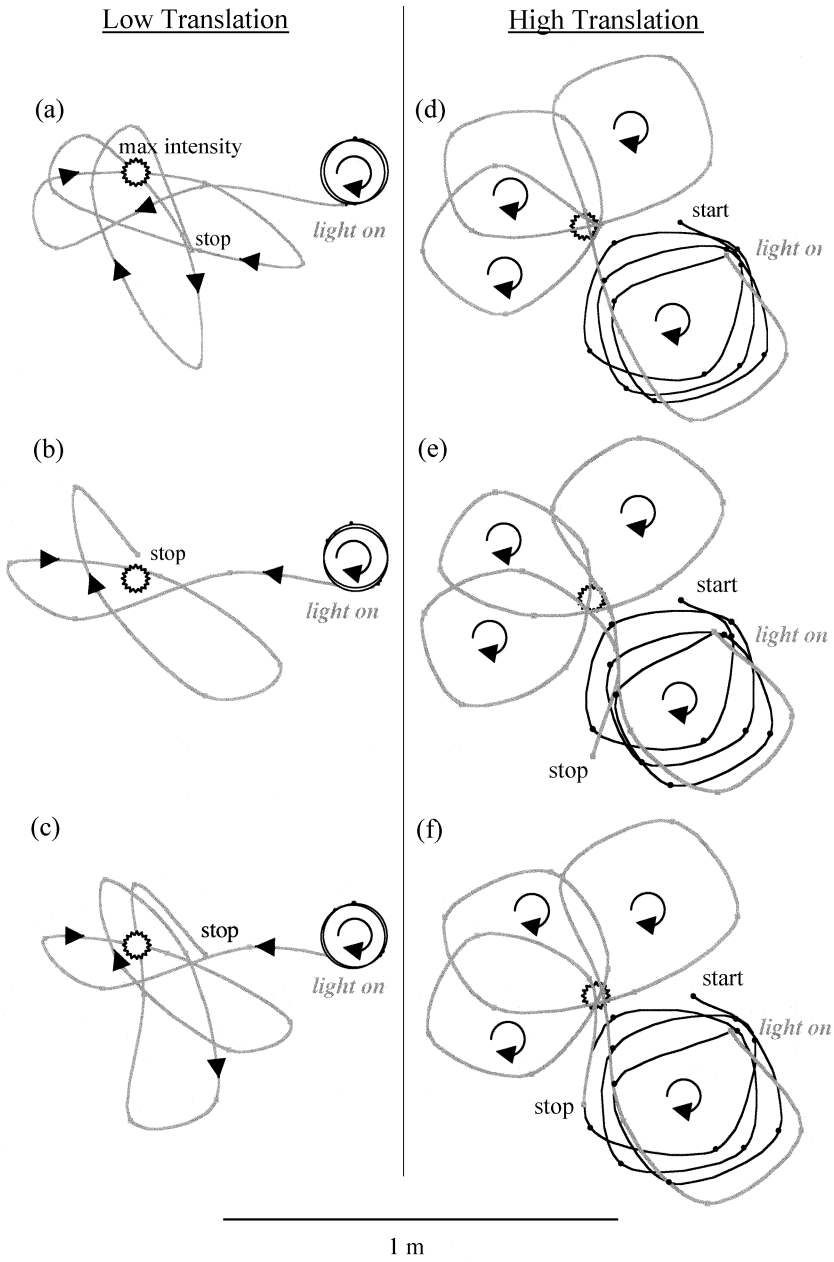

Fig. 5. Trajectories of the Rug Warrior under two different translational speeds, with start and stop positions indicated. The time when the light was turned on is indicated as the transition point from a black to gray line. The sun symbol shows the position on the surface of the floor of maximal light intensity. Arrowheads indicate forward motion, and curved arrows show the direction of rotation for a path section.

Solving (2) for $\omega = 0$, we found that the local heading was the sum of two angles. The first angle was the local direction of the field. The second angle was an offset which is a function of excitation intensity and sensor location δ

$$offset = \cos^{-1}\left(\frac{T_0}{f(r)}\right) - \delta. \tag{5}$$

For all runs, T_0 was held constant at 20. Equation (2) predicts the robot's behavior in a constant excitation field (see Section III)—the robot only orients to the vector field when the sensor placement δ is such that it nulls the offset. For a radial excitation field, the effect of the offset is more complex and is best understood geometrically. The source creates a 2-D field of headings that alone would drive the robot inwards. The effect of the offset is to rotate the heading that is actually followed by the robot. As (5) shows, the heading correction depends on both sensor placement δ and range.

In constant and spatially varying excitation fields, the robot's trajectory was obtained by numerically integrating the equations of motion. The spatially varying excitation field most closely models the "spotlight condition" used in the experiments with the embodied robots.

III. Results

A. Surface-Swimming Robotic Tadpole

The trajectories of the surface-swimming robotic tadpole in the control condition (control column, Fig. 4) were similar

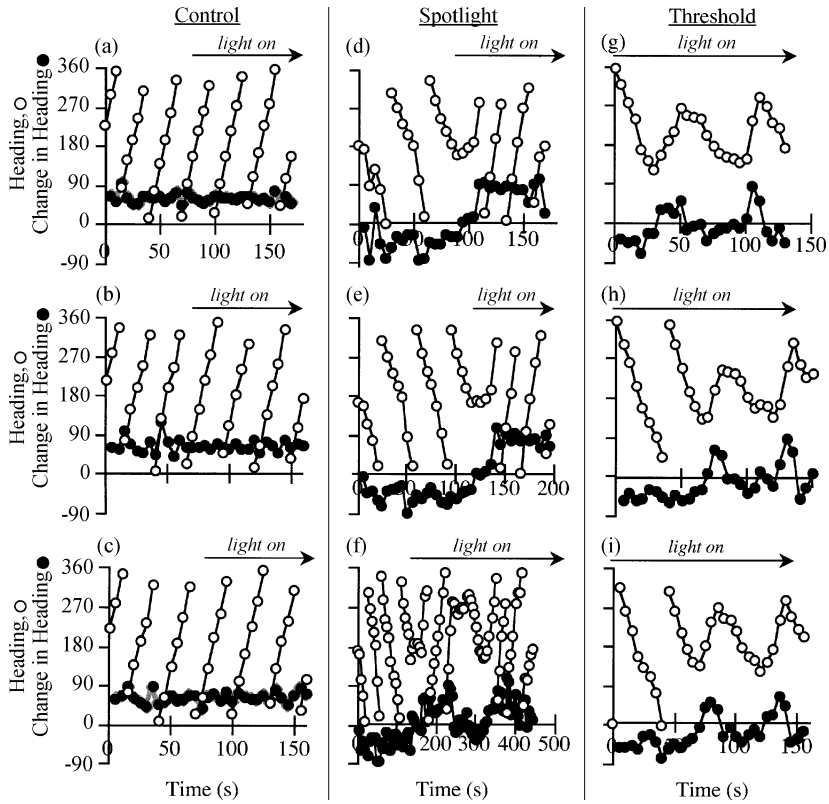

Fig. 6. Phototactic navigational behavior of the robotic tadpole as measured by robot heading (°, open circles) and change in heading with respect to time ("change in heading," ° per 5 s; filled circles). The control experiments (a)–(c) are compared to the two different experiments (d)–(i). The time when the light was switched on is indicated by the horizontal range of arrows. The behavioral response to light is indicated by a change in the slope of the heading line or a zero crossing of the change in heading line. The trials correspond to those shown in Fig. 4.

before and after the light was turned on—navigation up the light intensity gradient was absent. In contrast, once the robot had the cHK neural circuit turned on (Spotlight and Threshold condition columns, Fig. 4), the pre- and poststimulus behaviors were quite different. In all cases, the robotic tadpole headed toward the light source and then held station around the maximum intensity point. Please note that using only the 2-D cHK primitive, the robots cannot home and then stop at the source. With the 2-D cHK primitive, station holding, or more generally attraction to the source, is an adjustable function of the angular position of the sensor (see Section III).

When not in a light gradient, the location of the robotic tadpole was more evenly distributed spatially (Fig. 4). In the spotlight condition, the robot moved in clockwise loops that became small-radius counterclockwise loops when the stimulus was turned on. In the threshold condition, the robot spun in circles until it crossed the light threshold, at which point the robot headed up the light intensity gradient directly and held station, moving back and forth along the tank wall.

Examination of the heading θ and the change in heading ω (Fig. 6) quantifies what was qualitatively apparent from the robots' positional data. For the robotic tadpole, the control experiments showed little difference in ω through any of the trials, whereas the spotlight condition showed a distinct switch in ω from negative to positive after the stimulus was turned on. This indicates the change from clockwise to counterclockwise rotation that was observed (Fig. 4). In the threshold conditions, the heading shows how the robot went through 360° rotations once or twice before oscillating around a light-oriented heading. A strong correlation existed between the change in heading, ω and the light intensity detected by the photoresistor in the spotlight condition (Fig. 8). All linear regression lines were statistically significant $(\mathrm{p} < 0.05)$ with coefficients of determination (r^2) greater than 0.63.

B. Terrestrial Robot

The Rug Warrior's position in both high- and low-speed conditions (Fig. 5) showed clockwise spinning behavior until the stimulus was introduced. In response, the Rug Warrior headed toward the light source, and then held station in a series of clockwise loops that passed through the point of maximum intensity.

The change in heading ω for both conditions of the Rug Warrior (Fig. 7) remained steady until the stimulus was introduced, at which point the heading θ showed a series of straight runs and turns. While the same trend was present as seen in the robotic tadpole, in the Rug Warrior no significant correlation existed between the change in heading ω and the light intensity detected by the photoresistor in the spotlight condition. The variability in these data arises from the rapid motion of the robot and the delay in printing values on the LCD screen.

C. Simulated Robot

In a constant excitation field, when the sensor was pointed at $\delta = 45°$, a typical trajectory shows the simulated robot quickly turning toward its final heading and then translating with no further change in heading (Fig. 9). This behavior was as predicted

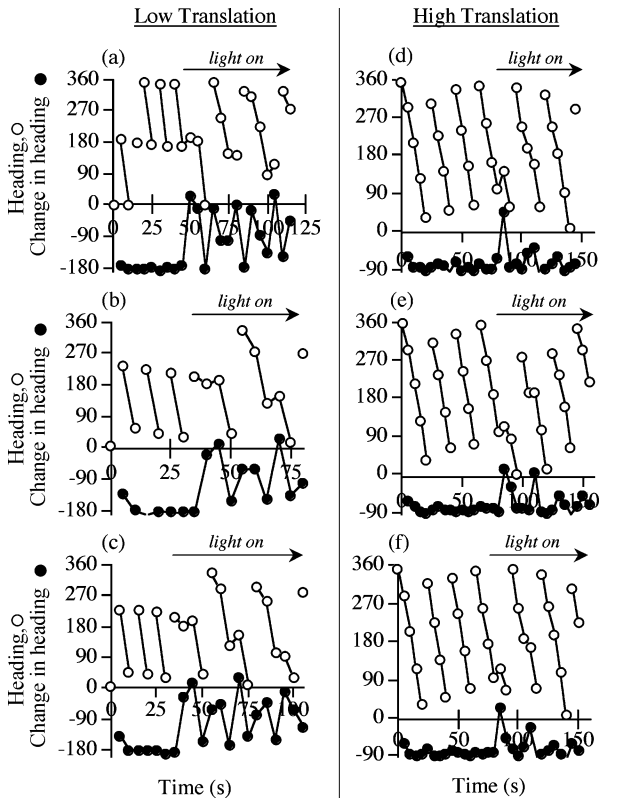

Fig. 7. Phototactic navigational behavior of Rug Warrior as measured by robot heading (degrees, open circles) and change in heading (° per 5 s; filled circles). Low translation and high translation programs are compared (left and right columns, respectively). The time when the light was switched on is indicated by the horizontal range of the arrows. Behavioral response to light is indicated by a change in the slope of the heading line or a zero crossing of the change in heading line. The trials correspond to those shown in Fig. 5.

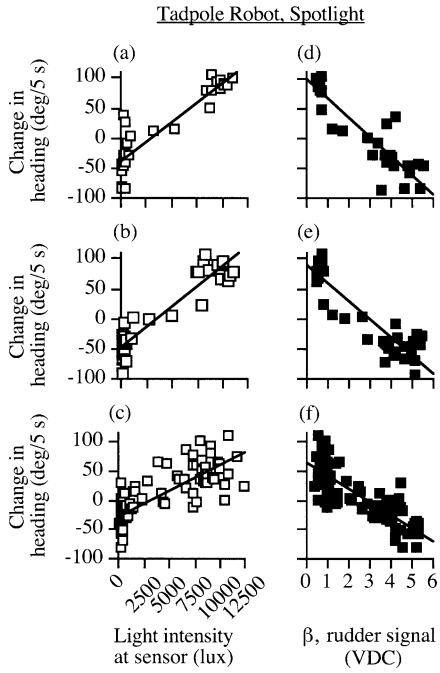

Fig. 8. Control of heading change. In the surface-swimming robotic tadpole (a)–(f), change in heading is directly proportional to the light intensity detected by the photoresistor. The connection between sensor and behavioral response is mediated by the computed rudder or lateral orientation signal, β. Lines are linear regressions (all $p < 0.05$). In the Rug Warrior (g)–(l), the same general patterns are seen even though the regression lines are not statistically significant in all cases. The pairs of figures in each row correspond to the trials shown in Figs. 4(d)-(f) and 6(d)-(f).

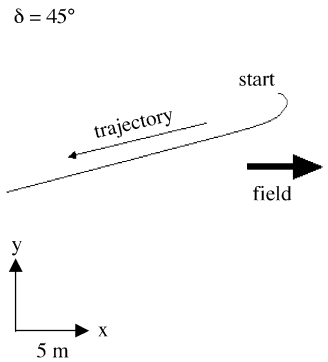

Fig. 9. Simulated 2-D cHK robot moving in a field of constant excitation (field direction indicated by thick arrow) with the sensor at the angle used in the embodied robots ($\delta = 45°$). Effective navigation toward the source does not occur in this excitation field. The simulation starts with the robot pointing in the direction of the field arrow at the positon marked "start." Parameters: $U = 0.2$ m·s^{-1}, $f(r) = 40$ r^{-1}, $T_o = 20$, and $\alpha = 0.005$.

by (5)—the robot quickly nulled its angular velocity ω, regardless of its initial orientation, at which point its motion became purely translational. Interestingly, the trajectory does not line up with the excitation field. As discussed in Section II, the asymptotic orientation relative to the excitation field depends on sensor location δ and on the ratio of signal over threshold intensity (5).

For a spatially varying excitation field, navigational behavior of the simulated robot varied dramatically with the placement angle of the sensor δ (Fig. 10). When the sensor was pointed forward, $\delta = 0°$, the heading correction only depended on signal intensity, was zero far from the source and was 90° near it. The total heading field was inwards away from the source and had a small rotational component near it. The trajectories generated by this heading field were attractive, and the simulated robot headed toward the source and then held station around it.

When the sensor was pointed aft, $\delta = 180°$, the heading field pointed outwards (Fig. 10). In this case, the source repelled the simulated robot, and it spiraled away.

When the sensor was pointed athwartships, $\delta = 90°$, the heading field pointed inwards with a strong rotational component near the source (Fig. 10). Near the source, the adiabatic approximation (see Section II) broke down because the field varied quickly; instead of being captured by the source, the robot passed close to it but then escaped. This phenomenon is best thought of as a form of inertia, and formally arises because of the finite duration of the memory kernel of the equations of motion.

When the sensor was pointed at $\delta = 45°$, the sensor angle that matched that in the embodied robots, the heading field pointed inwards with a rotational component near the source (Fig. 11). The simulated robot headed toward the source, passed closely to it (innermost circle), and then was captured, holding station in an outer orbit.

The dependence of the robot's 2-D cHK trajectory on sensor placement is also seen in 3-D cHK [3]. However, the similar behaviors have different origins. In 3-D cHK, the trajectories were determined by the phasing of the angular velocity changes with

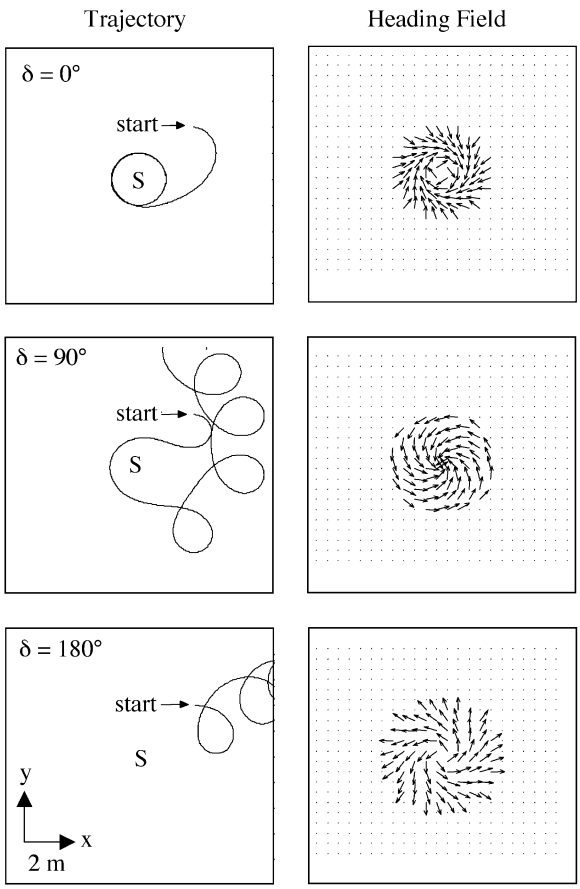

Fig. 10. Simulated 2-D cHK robot moving in a field of radial excitation, showing the influence of sensor position δ on trajectory and heading field. A range of navigational behaviors occur, from attractive positive phototaxis ($\delta = 0°$) to repulsive negative phototaxis ($\delta = 180°$). Intermediate sensor position ($\delta = 90°$) yields more complex behavior: initial attraction followed by repulsion and then large-orbit wandering. The simulation starts with the robot pointing in the direction and at the position of "start" arrow. The location of the source of the excitation field is denoted by "S." Parameters: $U = 0.2$ m·s^{-1}, $f(r) = 40$ r^{-1}, $T_o = 20$, and $\alpha = 0.01$.

respect to the source. In contrast, in 2-D cHK the kinematics were driven by the robot constantly adjusting its heading to null its angular velocity.

D. Comparison of Embodied and Simulated Robots

The trajectories of embodied (Figs. 4 and 5) and simulated (Fig. 11) robots showed similar behavior, responding to the excitation field by quickly heading to the source and then holding station around it. Note that the robots were not programmed to stop once the source was reached. Instead, station holding near the source is viewed as the successful, dynamic-state completion of the navigational behavior. Thus our embodied and simulated robots show effective navigation using a single sensor and the cHK neural control system.

While all robots headed to the source and held station, the station-holding behavior of each robot differed. Most notable was that, compared to the simulated robot, the embodied robots had orbits of more variable size and orientation. Sources of the variation included inertia, leeway from the keelless hull of the robotic tadpole, and slippage in the wheels of the terrestrial robot.

IV. Discussion

A. Neural Control of Single-Sensor Navigation in Robots

Using a laterally biased, flapping propulsion system similar to that seen in tadpole-like ascidian larvae, the autonomous surface-swimming robotic tadpole detected and oriented toward greater light intensity, navigated up the gradient, and held station in an orbit around the source of maximum light intensity (Fig. 4). In two different light environments, the robot's navigational behavior was controlled solely by modulation of the vehicle's rotational velocity ω (Fig. 6), a result consistent with predictions from 3-D HK theory [10], [11]. Rotational velocity, in turn, was controlled by an analog neural circuit that proportionally matched changes in light intensity at a single photoresistor to changes in the lateral orientation β of the flapping tail (Fig. 8), a result consistent with predictions from physics-based simulations of tadpole-like ascidiean larvae [7]. In terms of length-specific turning performance, the robotic tadpole outperforms real ascidian larvae, a fish-like robot, and a mini-AUV (Table I).

As our simulated robot shows (Fig. 10), navigational behavior in 2-D cHK is tuned primarily by the angular position of the sensor relative to the robot's centerline. While we have yet to test this variable experimentally, behavior of the simulated and embodied robots with a sensor angle of 45° (compare Figs. 3, 4, and 10) shows sufficient similarity to suggest that other behaviors, predicted when sensor angle varies, are likely to hold. An additional and important consequence of the mathematical model is that navigation can occur with many different kinds of sensors. Although we used a light intensity field, the same 2-D cHK primitive could be used to navigate with respect to 1) the earth's magnetic field using a one-axis magnetometer, 2) the gravitational field using a one-axis accelerometer, 3) an acoustic source using a single transducer, or 4) an electric field using an electrometer.

B. Engineering Opportunities With 2-D cHK

For engineers, our most important result is that the simple, single-sensor navigational schema proposed for small, tadpole-like ascidian larvae [7] works in aquatic and terrestrial robots operating in 2-D. Cycloptic 2-D HK is a new navigational primitive, inspired from biological systems, available for implementation in analog or digital systems to allow autonomous vehicles to orient, navigate, and hold station.

Two different approaches to implementation of 2-D cHK are possible: 1) as a behavioral control module—use of 2-D cHK as a schema, that is, as a module nested within a more complex behavior-based robotic architecture [1] and 2) as an autonomous vehicle primitive—use of 2-D cHK as a complete robotic agent as demonstrated in this paper.

Use of 2-D cHK as a behavioral control module within an existing autonomous vehicle offers several attractive features: a) single sensor operation—provides redundancy in two-sensor systems, where failure of one sensor could activate cHK to extend mission time or aid in vehicle recovery, b) low control costs—cHK navigation is simple to implement algorithmically, allowing cheap analog or quick computational control, and c)

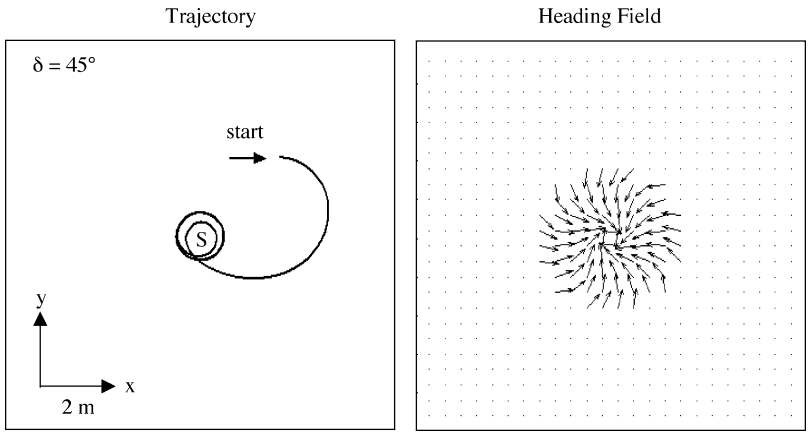

Fig. 11. Simulated 2-D cHK robot moving in a field of radial excitation, showing navigational behavior with sensor at the angle used in the embodied robots ($\delta = 45°$). As seen in the embodied robots, the simulated robot detects the source (labeled "S"), navigates toward it, and then holds station around it. Farther away from the source the heading field is oriented inwards, toward the source. At distances closer to the source, the heading field is rotational. The simulation starts with the robot pointing in the direction and at the position of "start" arrow. Parameters: $U = 0.2$ m·s^{-1}, $f(r) = 40$ r^{-1}, $T_o = 20$, and $\alpha = 0.01$.

TABLE I
COMPARISON OF THE LOCOMOTOR PERFORMANCE OF AUTONOMOUS AQUATIC AGENTS

Parameter	tadpole-like larva, *Aplidium constallatum*[1]	robotic tadpole[2]	robotic carangiform fish[3]	Ranger^{TM} microUUV[4]
body length (m)	0.0025	0.357	0.483	0.92
tailbeat frequency (Hz)	25.2	2	2.2	n/a
speed (m s^{-1})	0.0143	0.034	0.638	1
normalized speed (lengths s^{-1})	6.35	0.095	1.321	1.09
curvature of trajectory (rad m^{-1})	750	34.38	0.16	0.67
normalized curvature of trajectory (rad body length^{-1})	1.67	12.28	0.08	0.73
tailbeats to change heading 45°	41	19	25	n/a
duration 45° heading change (s)	1.62	1	n/a	n/a
number of gradient-relevant sensors used	1	1	1	2
kinematic DOF	1	1	1	2

[1] Mean values from [6].
[2] Mean values from this study.
[3] Mean values from [20], using data from turning with caudal fin only.
[4] Mean values from [21]. Curvatures are maximal turning performance.

vehicle instability tolerance—since cHK acquires gradient information directly from its movement interaction with the environment, platform wobble is subsumed in the continuous perception-action calculation.

The most important feature of behavioral implementation is that cHK can operate on any system with a thruster and a rudder. Thus existing vehicles would not require substantial retrofitting to make 2-D cHK operational. All that is needed is either a) a digital algorithm linking a sensor of choice to rudder angle (see Section II) or b) a parallel backup analog controller (see Fig. 3). If failure of the main guidance system occurs, the analog backup controller could initiate planar station-holding by use of any number of single sensors (see previous section). Depth maintenance, or automatic surfacing, would need to be a separate, parallel backup module.

As a vehicle primitive, the 2-D cHK system offers simple construction, requiring only a single propulsor and sensor, features more conducive to the miniaturization of robotic vessels than designs with paired sensors and propulsors. However, from an application standpoint, assessment depends on usefulness, size, simplicity, and cost. The value of 2-D cHK is that it permits aligning to a vector field using a single actuator, which reduces cost and size, and improves overall electromechanical simplicity. For 3-D navigation, it has been shown that 3-D cHK vehicles find a niche in applications that require vehicles so small that only one actuator fits in the hull. We suggest the same conclusion for 2-D cHK.

While 2-D cHK would seem inappropriate for AUVs operating in 3-D, in roll-stable platforms, the planar control could be combined with an independent depth control, allowing the ve-

hicle to navigate at a given depth using 2-D cHK. On the other hand, depth control could be established as an orthogonal 2-D cHK system operating in pitch rather than yaw. With appropriate constraints on pitch range, the combined 2-D cHK system could provide effective 3-D navigation. Two reasons for choosing the hybrid 2-D-3-D cHK system over a true 3-D HK one [14] would be a) if roll stability were a design constraint or b) if two separate vector fields, say light and depth, were being simultaneously sampled and a fused behavioral output, the summation of independent vector field responses [1] were desired.

C. Research Tool

Robotic systems provide a tool for testing agent-behavior hypotheses generated from computer simulations and from biological systems [17]. The use of robotic systems for this purpose is the source of much current debate [18]. For workers interested in testing agent control theory in cognitive science and artificial intelligence, the simplicity of the 2-D cHK system offers several important opportunities. First, for navigation in a vector sensory field, it is difficult to imagine a simpler system for planar motion than that instantiated in the aquatic and terrestrial robotic systems. Even the seminal Braitenberg vehicles rely, for planar navigation, on two sensors and two independent motor outputs [19]. In contrast, 2-D cHK systems use only one sensor, control kinematics with a single degree of freedom, and do not make temporal comparisons. Thus the 2-D cHK primitive can be exploited as a limiting condition for testing theory related to behavioral emergence in agent-environment interactions [1]. Second, as an autonomous vehicle, the 2-D cHK robotic system can easily be adapted for multi-agent research. There is a growing community studying robotic swarming and other bioinspired group behaviors which rely on the assumption of hundreds of vehicles. Robotic platforms are unfortunately expensive (typically, a single vehicle is priced in the range $10 000 to $200 000), and essentially all work to date has been done in simulations. 2-D and 3-D cHK robots open the way to an inexpensive solution: because of their electromechanical simplicity, a cHK vehicle could cost much less than existing robotic platforms. As our simulations showed (Fig. 10) 2-D cHK enables three behaviors: movement toward a source, movement away from a source, and random walking. In combination, these three behaviors are sufficient for multiagent applications, and could be arbitrated in a subsumption hierarchy, for example. Complex collective motion can be achieved by placing a sensor *and* an emitter on each vehicle, enabling vehicle-vehicle interaction. With a swarm of interacting 2-D cHK vehicles, a variety of interesting agent ecologies could be produced.

V. Conclusion

We identified, modeled, and tested a biologically inspired behavioral primitive that allows planar navigation with a single sensor coupled to a single degree-of-freedom motor control. The navigational primitive—which we call 2-D cycloptic helical klinotaxis (2-D cHK)—was implemented in an autonomous surface-swimming robot. The surface-swimming robot detected a light intensity gradient, navigated up the gradient, and then held station at an orbital around the point of greatest intensity. The 2-D cHK navigational primitive was also tested in an autonomous terrestrial robot, which showed similar behaviors. Finally, the navigational primitive was used to mathematically simulate single-sensor robots. The navigational behavior of the simulated robot was a function of the angle of the single sensor relative to the body's centerline and the nature of the sensory excitation field. When the simulated and embodied robots had the same sensor angle (45°) and spatially varying excitation field (radial), they showed similar navigational behavior. Based on the evidence from embodied and simulated robots, we conclude that 2-D cHK is a robust navigational primitive for the control of planar motion in autonomous robots.

Acknowledgment

The authors thank P. Bandyopadhyay for his work as Editor of this volume and his leadership in promoting biorobotics while a program officer at the Office of Naval Research. Three anonymous reviewers provided helpful comments. C. Bertsche, J. Vanderlee, and E. Stout of Vassar College's Science Technology Support Department deserve thanks for their help building the robotic tadpole. L. Voerman and B. Suter were instrumental in early prototyping. K. Livingston served as robotics mentor to JHL and ACL. M. Quimb was a source of continual inspiration.

References

[1] R. C. Arkin, *Behavior-Based Robotics*. Cambridge, MA: MIT Press, 1998.

[2] R. R. Murphy, *Introduction to AI Robotics*. Cambridge, MA: MIT Press, 2000.

[3] M. Kemp, "Micro-AUVs II: Control," in *Proc. 12th Unmanned Untethered Submersible Technology*, Autonomous Undersea Systems Institute, Lee, NH, 2001.

[4] M. Kemp, H. Crenshaw, B. Hobson, J. Janet, R. Moody, C. Pell, H. Pinnix, and B. Schulz, "Micro-AUVs I: Platform design and multi-agent system development," in *Proc. 12th Unmanned Untethered Submersible Technology*, Autonomous Undersea Systems Institute, Lee, NH, 2001.

[5] M. J. McHenry, "Mechanisms of helical swimming: Asymmetries in the morphology, movement and mechanics of larvae of the ascidian *Distaplia occidentalis*," *J. Exp. Biol.*, vol. 204, pp. 2959–2973, 2001.

[6] M. J. McHenry and J. Strother, "The kinematics of phototaxis in larvae of the ascidian *Aplidium constellatum*," *Mar. Biol.*, vol. 142, pp. 173–184, 2003.

[7] J. A. Strother and M. J. McHenry, "How do marine invertebrate larvae orient to light? A numerical simulation of phototaxis in ascidian larvae," *Integ. Comp. Biol.*, vol. 42, p. 1320, 2002.

[8] G. Fraenkel and D. L. Gunn, *The Orientation of Animals: Kineses, Taxes and Compass Reactions*. New York: Oxford, 1940.

[9] H. C. Crenshaw, "Kinematics of helical motion of microorganisms capable of motion with four degrees of freedom," *Biophys. J.*, vol. 56, pp. 1029–1035, 1989.

[10] ——, "Orientation by helical motion. I. Kinematics of the helical motion of microorganisms with up to six degrees of freedom," *Bull. Math. Biol.*, vol. 55, pp. 197–212, 1993.

[11] ——, "Orientation by helical motion. III. Microorganisms can orient to stimuli by changing the direction of their rotational velocity," *Bull. Math. Biol.*, vol. 55, pp. 231–255, 1993.

[12] ——, "A new look at locomotion in microorganisms: Rotating and translating," *Amer. Zool.*, vol. 36, pp. 608–618, 1996.

[13] H. C. Crenshaw, C. N. Ciampaglio, and M. J. McHenry, "Analysis of the three-dimensional trajectories of organisms: estimates of velocity, curvature and torsion from positional information," *J. Exp. Biol.*, vol. 203, pp. 961–982, 2000.

[14] C. A. Pell, H. Crenshaw, J. Janet, and M. Kemp, "Devices and methods for orienting and steering in three dimensional space," US patent 6 378 801, Apr. 30, 2002.

[15] M. J. McHenry, E. Azizi, and J. A. Strother, "The hydrodynamics of locomotion at intermediate Reynolds numbers: undulatory swimming in ascidian larvae (*Botrylloides* sp.)," *J. Exp. Biol.*, vol. 206, pp. 27–343, 2003.
[16] D. Zwillinger, *Handbook of Differential Equations*, 3rd ed. New York: Academic, 1998.
[17] B. Webb, "Robots in invertebrate neuroscience," *Nature*, vol. 417, pp. 359–363, 2002.
[18] ——, "Can robots make good models of biological behavior," *Behav. Brain Sci.*, vol. 24, pp. 1033–1050, 2001.
[19] V. Braitenberg, *Vehicles: Experiments in Synthetic Psychology*. Cambridge, MA: MIT Press, 1984.
[20] K. A. Morgansen, "Geometric methods for modeling and control of a free-swimming carangiform fish robot," in *Proc. 13th Unmanned Untethered Submersible Technology*, Autonomous Undersea Systems Institute, Lee, NH, 2003.
[21] B. Schulz, B. Hobson, M. Kemp, J. Meyer, R. Moody, H. Pinnix, and M. St. Clair, "Multi-UUV missions using ranger microUUVs," in *Proc. 13th Unmanned Untethered Submersible Technology*. Lee, NH, 2003.

John H. Long, Jr. (M'04) received the B.A. degree in human ecology, with emphasis in functional morphology, from the College of the Atlantic, Bar Harbor, ME, in 1986 and the Ph.D. degree in zoology, with emphasis in biomechanics, from Duke University, Durham, NC, in 1991.

He is currently a Professor in the Department of Biology and the Programs in Neuroscience and Behavior and Cognitive Sciences at Vassar College, Poughkeepsie, NY. Previously, he was Assistant and then Associate Professor, having joined the Faculty in 1991. His current research interests include biorobotics and the evolution, mechanics, and control of propulsive systems in aquatic vertebrates. Since 1997, he has participated in the Unmanned Untethered Submersible Technology biannual meetings.

Dr. Long is a member of the Society for Integrative and Comparative Biology, the International Society of Vertebrate Morphology, the Society of Vertebrate Paleontology, and Sigma Xi.

Adam C. Lammert received the B.A. degree in cognitive science, with emphasis in robotics, from Vassar College, Poughkeepsie, NY, in 2004. He is pursuing the Ph.D. degree in computer science at North Carolina State University, Raleigh.

In 2002, he began his research career working in the Contextual Vocabulary Acquisition project at the State University of New York at Buffalo. He wrote his senior thesis on an extension of the work published here. His research interests include robotics and artificial intelligence.

Mr. Lammert is a member of the Society for Integrative and Comparative Biology and Psi Chi. In 2003, he received a Fellowship to the Undergraduate Research Summer Institute at Vassar College to work on robotics. He received Teaching Assistantships for two years in the Cognitive Science Program at Vassar College.

Charles A. Pell received the M.F.A. degree in sculpture from the University of Notre Dame, Notre Dame, IN, in 1987 and the B.F.A. degree in kinetic sculpture from Western Michigan University, Kalamazoo, in 1984.

He is a Founder and Director of Science and Technology for Nekton Research, LLC, Durham, NC, and an Associate in Research in the Biology Department, Duke University, Durham. From 1990 to 1997, he was Art Director of the Bio-Design biomechanics modeling facility within the Department of Zoology at Duke University. Prior to that he was Coordinator of Research for Dinamation International Corporation in San Juan Capistrano, CA. His current research interests include biomimetic autonomous undersea robots and related systems, the functional morphology of fluid locomotion, soft tissue force transmission systems, and novel methods for physically modeling biological systems. He has received four patents covering robotics, propulsion, and guidance technologies.

Mr. Pell is a member of the Society for Integrative and Comparative Biology, Sigma Xi, the American Association for the Advancement of Science, and BLIMP.

Mathieu Kemp received the B.Ing. degree in engineering physics from Ecole Polytechnique de Montreal in 1986, the M.Sc.A. degree in applied physics from Ecole Polytechnique de Montreal in 1988, and the Ph.D. degree in physics from the University of North Carolina at Chapel Hill, in 1992.

He is currently Director of Physics at Nekton Research, LLC, Durham, NC. He has held appointments at Duke University, Northwestern University, Universidad de Los Andes, and Ecole Polytechnique de Montreal.

Dr. Kemp is a member of the American Association for the Advancement of Sciences and the Institute of Navigation.

James A. Strother received the B.A. degree in physics, with emphasis in biomechanics, from the University of California, Berkeley, in 2004.

He was a Research Assistant in the Department of Integrative Biology, University of California, Berkeley.

Mr. Strother is a member of the Society for Integrative and Comparative Biology.

Hugh C. Crenshaw received the B.A. degree in biology from Davidson College, Davidson, NC, and the Ph.D. degree in zoology, with emphasis in biomechanics, from Duke University, Durham, NC.

He is currently Director of Technology Development at GlaxoSmithKline, Research Triangle Park, NC. He is a Founder of Nekton Research, LLC, Durham, and was previously a Research Professor at the Pratt School of Engineering, Duke University, after being an Assistant Professor in the Zoology Department of Duke University.

Matthew J. McHenry received the B.A. degree in art and in biology from Vassar College, Poughkeepsie, NY, in 1995 and the Ph.D. degree in integrative biology, with emphasis in animal biomechanics, from the University of California, Berkeley, in 2002.

He is currently a National Science Foundation Postdoctoral Fellow at Harvard University, Cambridge, MA, working on the hydrodynamics of swimming in larval fish. He will join the University of California, Irvine, as an Assistant Professor.

Dr. McHenry is a member of Sigma Xi, the American Society of Limnology and Oceanography, the American Society of Biomechanics, the International Society of Vertebrate Morphologists, the Society for Experimental Biology, and the Society for Integrative and Comparative Biology.